

Antiferromagnetic order without recourse to staggered fields

H. C. Donker*

Radboud University, Institute for Molecules and Materials, Heyendaalseweg 135, NL-6525AJ Nijmegen, The Netherlands

H. De Raedt

Zernike Institute for Advanced Materials, University of Groningen, Nijenborgh 4, NL-9747AG Groningen, The Netherlands

M. I. Katsnelson

Radboud University, Institute for Molecules and Materials, Heyendaalseweg 135, NL-6525AJ Nijmegen, The Netherlands

(Received 30 April 2018; revised manuscript received 21 June 2018; published 16 July 2018)

In the theory of antiferromagnetism, the staggered field—an external magnetic field that alternates in sign on atomic length scales—is used to select the classical Néel state from a quantum magnet but justification is missing. This work examines, within the decoherence framework, whether repeated *local* measurement can replace a staggered field. Accordingly, the conditions under which local decoherence can be considered a continuous measurement are studied. The dynamics of a small magnetic system is analyzed to illustrate that local decoherence can lead to (symmetry-broken) order similar to order resulting from a staggered field.

DOI: [10.1103/PhysRevB.98.014416](https://doi.org/10.1103/PhysRevB.98.014416)**I. INTRODUCTION**

The decoherence program intends to clarify the emergence of classical physics from within quantum mechanics. The standard works [1–3] follow essentially a bottom-up approach in which the decoherence of a single particle (e.g., a quantum Brownian particle or a single spin) is discussed. Although this clarifies the fragility of quantum states of different macroscopic configurations, it does not explain how a genuine many-body system, whereby the local particles are inextricably quantum correlated (i.e., entangled), can turn into a collection of classical particles. Motivated by the prospects of quantum information technology, developments in the understanding of the decoherence of bi- and multipartite entangled systems are only now beginning to unfold [4–8]. However, subtleties relating to classicality are, to the best of our knowledge, still largely unexplored. Nevertheless, in the context of magnetism, several works attempted to tackle this problem by truncating a many-body magnet to a two-level system [9–13]. In particular, Prokof'ev and Stamp reviewed in detail the effects of a spin environment on a two-level system [9,10], for which a mapping to the spin-boson model [14] can in general not be made. (See also a complementary review [15] that analyzes a two-level system in a spin environment from a numerical perspective.)

On the other hand, large systems lead to emergent collective properties that are difficult to understand from a simplified sum-of-its-parts view, as discussed in several popular scientific accounts [16–18]. Indeed, the concept of spontaneous symmetry breaking, in which solutions are singled out in the thermodynamic limit by infinitesimal fields, depend on the (collective) low-energy behavior of a macroscopic system [19,20]. Most systems break a(n almost) continuous symmetry—like the

direction or location in space—and therefore require a host of states which conspire to form localized structures; a two-level description is then, by its very nature, inadequate.

What is more, a symmetry-breaking analysis indicates *if* such solutions can be singled out but does not address the *how*, i.e., the physical mechanism that is responsible.

In magnetism, for example, this difficulty comprises the (in)consistency of the (classical) Néel state $|\psi_N\rangle$ (the state in which neighboring spins align antiparallel $|\uparrow\downarrow\uparrow\dots\rangle$ or vice versa) with the antiferromagnetic Heisenberg Hamiltonian (HH) [21,22], its experimental evidence [23], and the possible physical realization of the staggered field (explained below). The problem is as follows: The exact ground state (GS) $|\psi_0\rangle$ of the antiferromagnetic HH

$$H = J \sum_{(i,j)} \mathbf{S}_i \cdot \mathbf{S}_j \quad (1)$$

is known to be a total spin $S_{\text{tot}} = 0$ singlet [24], whereby the local magnetization of each spin S_i vanishes $\langle\psi_0|\mathbf{S}_i|\psi_0\rangle = 0$ according to group theory (see, e.g., the Wigner-Eckart theorem [25]). In this equation, the exchange constant J is positive and the sum extends over nearest neighbors. Contrary to the GS, the Néel state $|\psi_N\rangle$ is not an eigenstate of the HH and is thus a very specific linear combination of a (possibly extensive [26] number of) spin S_{tot} states. Moreover, the sublattice magnetization is not a constant of motion. Therefore, the sublattice magnetization of an arbitrary state, including the Néel state, will decay. However, since the energy levels close to the GS are very nearly degenerate, collapsing onto the GS as $1/N$ with N being the number of particles [27], the decay rate can be rather long. Anderson estimated the time for the Néel state to rotate to an orthogonal direction to be roughly three years [27]. Furthermore, the actual GS energy E_0 is bounded

*h.donker@science.ru.nl

quite strongly [22,28],

$$-\frac{1}{2}NJZS_i^2 > E_0 > -\frac{1}{2}NJZS_i^2[1 + 1/(ZS_i)], \quad (2)$$

with S_i being the single-site spin (which is taken to be the same for all i), and Z being the coordinate number of the lattice. In the limit $1/(ZS_i) \rightarrow 0$, the GS energy E_0 precisely coincides with the energy of the Néel state [left-hand side of Eq. (2)].

A mathematical trick to overcome the inconsistency between the Néel state $|\psi_N\rangle$ and the nondegenerate singlet $|\psi_0\rangle$ introduces a staggered field, $\mathbf{M} = \mathbf{S}_A - \mathbf{S}_B$ (the order parameter), with opposite signs on sublattices A and B , that couples to a conjugate field, \mathbf{h}_{st} . Time-reversal invariance is thus explicitly broken by adding the term $H_{\text{st}} = \mathbf{M} \cdot \mathbf{h}_{\text{st}}$ to the Hamiltonian. The sublattice magnetization then arises as a quasiaverage [29], whereby the conjugate field \mathbf{h}_{st} tends to zero after taking the thermodynamic limit. Although it is known that an effective staggered field can be generated in very specific crystal structures [30], it is usually regarded as unphysical [20,23,31,32]. More generally, the proper choice of the order parameter cannot always be decided *a priori*, but is dictated by phenomenology [33].

Assume now, for the sake of argument, that the staggered field does have a physical origin. For naturally occurring magnetic fields of arbitrary shape that are infinitely differentiable, the Fourier component corresponding to the staggered field is suppressed faster than any power of the spectral scale (which is typically much larger than the lattice spacing) and hence decreases superexponentially below this scale. Therefore, arbitrary stray fields emanating from outside into the sample are an unlikely source of the staggered field.

In fact, for the interpretation of neutron diffraction experiments no such field is required [23,34,35]. Elastic neutron diffraction experiments probe the time-reversal invariant static structure factor [Eq. (22)] and therefore do not require symmetry-broken states [23,34,35]. An explicit demonstration was given by Irkhin and Katsnelson [23], who proposed a trial wave function *without* broken symmetry for the Heisenberg antiferromagnetic model in the semiclassical $1/(ZS_i) \rightarrow 0$ limit. Not only were they able to reproduce the peaks at the antiferromagnetic reciprocal lattice vector in the static structure factor, but also the nuclear magnetic resonance line form could be accounted for without resorting to broken symmetry.

Besides the existence and necessity of the staggered field, it is *a priori* unclear whether this mathematical trick indeed leads to nonvanishing anomalous averages $\langle \mathbf{M} \rangle \neq 0$ upon sending $\mathbf{h}_{\text{st}} \rightarrow 0$ after taking the thermodynamic limit. The Lieb-Mattis model [24] is one of the few nontrivial systems where this can be worked out in detail [36,37]. More generally, the ability to develop spontaneous staggered magnetization hinges on the presence of long-range order. In the antiferromagnetic Heisenberg model on the cubic lattice, long-range order was first established by Dyson et al. [38] for $d \geq 3$ spatial dimensions and spin $S_i \geq 1$. This proof was later strengthened by others for $d = 3$ to include the case $S_i = 1/2$ [39]. In two spatial dimensions, numerical evidence suggests long-range order in the GS for both the bipartite [35,40,41] and the triangular lattice [41–44] when $S_i = 1/2$ (for other lattices, see also Refs. [35] and references therein). Only fairly recently was it demonstrated that taking an anomalous average does indeed

lead to broken symmetry for the HH on a bipartite lattice, provided that long-range order exists [45,46].

Later refinements of several experimental techniques called for a reevaluation of the magnetic ordering in antiferromagnets. Measurements of the quadrupole magnetic moment of the antiferromagnetic compound Cr_2O_3 indicated broken symmetry in the magnetic structure [47]. Furthermore, state-of-the-art spin-polarized scanning tunneling microscopy (STM) experiments can probe the magnetization of individual atoms and have revealed antiferromagnetic structures whereby time-reversal symmetry is manifestly broken. Moreover, these structures have been seen to telegraph between the two alternating Néel configurations [48,49], reminiscent of Bohr's quantum jumps in atoms [1]. (In these works [48,49], they considered $S = 2$ Fe atoms on Cu_2N that have a large magnetic easy-axis anisotropy [50] which consequently suppresses quantum fluctuations.) This has sparked renewed interest in how such classical magnetic order can come about from quantum systems [11–13]. This work contributes to the discussion by analyzing the necessity of the staggered field, going beyond a two-level simplification.

Historically, the decoherence program focused primarily on single-particle subsystems but, as it turned out, the decoherence of local particles in a many-body subsystem can lead to many surprising consequences. Examples are the decoherence wave [51–53], suppression of the Kondo effect [54,55], and the creation of sublattices in antiferromagnets [56], all of which considered idealized local measurement (i.e., a wave function collapse). This work follows up on a suggestion in Ref. [56] that repeated local measurements on antiferromagnets can replace a staggered field. A decoherence approach is followed, in which the entanglement between a local spin of an antiferromagnet and an environment is studied. Since the decoherence process is technically different from wave function collapse, first a detailed comparison is carried out. Next, a critical assessment is made to clarify under which conditions, and to what extent, the repeated measurement hypothesis is correct with the help of numerical calculations.

For clarity, the analysis is broken up in two parts. In model A, the decoherence of a local particle is compared to idealized measurement (Sec. III). In model B, local decoherence is applied to a low-energy description of antiferromagnets (Sec. IV). Both models are outlined in Sec. II and implications are discussed in Sec. VI.

II. OUTLINE MODELS

The two spin models that are the centerpiece of this work shall now be outlined. Units in which the reduced Planck constant \hbar and the Boltzmann constant k_B equal unity are used throughout this paper. In both models, the entire system consists of a collection of spin-1/2 particles. A single (local) particle is strongly coupled to an environment along the z direction, so as to resemble a measurement-like interaction. While model A mainly serves to compare ideal measurement with local decoherence, model B extends the environment of A by introducing a thermal reservoir. An important difference between models A and B is that in the latter an effective description of antiferromagnets is used (for a detailed discussion, see

Sec. IV) for the system of interest [henceforth, central system (CS)].

A. Model A: Decoherence of a local spin

The entire system is partitioned in two parts, the CS (denoted by S) and its complement, the environment (indicated by \mathcal{E}). The CS (environment) is composed of $N_S = 6$ ($N_{\mathcal{E}} = 8$) spin-1/2 particles. To avoid unnecessarily complicating the analysis, the CS with Hamiltonian H_S^- interacts locally with environment \mathcal{E} via H_I , while the spins in \mathcal{E} have no Hamiltonian of their own. That is, the intraenvironment Hamiltonian (the self-Hamiltonian of \mathcal{E}) is neglected. The Hamiltonian of model A can then be written as

$$H_A = H_S^- + H_I. \quad (3)$$

The CS is taken to be an open chain of N_S spins (i.e., $S_i = 1/2$ for all i), coupled via Heisenberg exchange [22]

$$H_S^- = J_S \sum_{i=1}^{N_S-1} \mathbf{S}_i \cdot \mathbf{S}_{i+1}, \quad (4)$$

with exchange constant J_S , and the $-$ superscript indicates the lattice geometry (in this case, an open chain). To emulate decoherence as a *measuring* effect on a local spin, which is chosen to be spin S_1 , requires a well-defined measurement direction. The z axis is selected such that the system-environment interaction takes the following form:

$$H_I = I \sum_{i \in \mathcal{E}} r_i S_1^z S_i^z \equiv I S_1^z \tilde{S}_{\mathcal{E}}^z, \quad (5)$$

where the sum is over all $N_{\mathcal{E}}$ spins inside the environment \mathcal{E} , I is the interaction strength, $\{r_i\}$ are a set of random numbers $r_i \in [0, 1]$, and $\tilde{S}_{\mathcal{E}}^z = \sum_{i \in \mathcal{E}} r_i S_i^z$. The use of random numbers are to suppress recurrences of phase coherence after the initial Gaussian decay. In order for \mathcal{E} to couple strongly to the CS, I is set to $I = 20J_S$.

B. Model B: Addition of a thermal reservoir

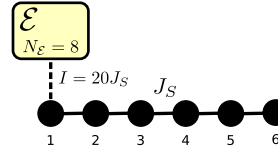
In model B, the CS interacts with an environment \mathcal{E} , but in this case \mathcal{E} consists of two fragments \mathcal{E}_1 and \mathcal{E}_2 . Fragment \mathcal{E}_1 describes the strong decoherence with the local spin, while \mathcal{E}_2 couples weakly to the entire CS to mimic contact with a thermal reservoir. The Hamiltonian of model B is split into four,

$$H_B = H_S^{\circ} + H_{I_1} + H_{I_2} + H_{\mathcal{E}_2}, \quad (6)$$

with H_S° being the Hamiltonian of the CS (the \circ indicates ring geometry), H_{I_1} (H_{I_2}) being the coupling between the CS and \mathcal{E}_1 (\mathcal{E}_2), and $H_{\mathcal{E}_2}$ being the self-Hamiltonian (i.e., the intraenvironment Hamiltonian) of \mathcal{E}_2 . A schematic of the setup is shown in Fig. 1. The Hamiltonian, H_S° , is given by Eq. (4) with the addition of the boundary term $H_S^{\circ} = H_S^- + J_S \mathbf{S}_1 \cdot \mathbf{S}_{N_S}$, thereby giving rise to a ring geometry.

Similar to model A, spin S_1 of the CS is strongly coupled to spins in \mathcal{E}_1 via Ising coupling. H_{I_1} is identical to Eq. (5), apart from the sum that is now restricted to the $N_{\mathcal{E}_1}$ sites pertaining to fragment \mathcal{E}_1 .

Model A



Model B

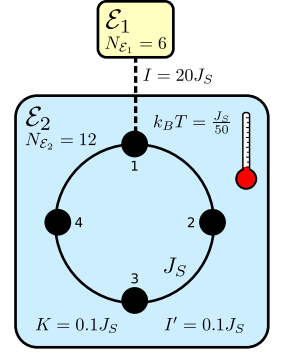


FIG. 1. Schematic of models A and B. In model A (B), the central system consists of an open (periodic) chain of $N_S = 6$ ($N_S = 4$) spin-1/2 particles and spin S_1 is strongly coupled to an environment \mathcal{E} (environment fragment \mathcal{E}_1) of spins via Ising coupling. In model B, the spin chain is immersed in fragment \mathcal{E}_2 that resembles a thermal reservoir (inverse temperature $\beta = 50/J_S$). The number of spins in each environment (fragment) and the respective coupling strengths are indicated in the figure.

For \mathcal{E}_2 , slightly different system-environment couplings are used to facilitate decoherence of the energy states. In Ref. [57], it was found that binary coupling strengths and the presence of a conserved quantity are particularly efficient. Therefore, the following coupling to \mathcal{E}_2 is chosen,

$$H_{I_2} = \sum_{i \in S, k \in \mathcal{E}_2} I'_{ik} S_i^z S_k^z, \quad (7)$$

where i runs over spin indices in the CS (indicated by S) and I'_{ik} are binary values $\pm I'$ picked at random. As for the self-Hamiltonian of \mathcal{E}_2 , spin-glass-like couplings are used to maximize decoherence and relaxation [57,58]

$$H_{\mathcal{E}_2} = \sum_{\alpha \in \{x, y, z\}} \sum_{k, l \in \mathcal{E}_2} K_{kl}^{\alpha} S_k^{\alpha} S_l^{\alpha}, \quad (8)$$

with K_{lm}^{α} being uniform random numbers in the range $[-K, K]$. The philosophy behind the specific form $H_{\mathcal{E}_2}$ is that it is not necessary to have a very large environment in order to have efficient decoherence and relaxation [57,58], thereby keeping the problem computationally tractable. But this comes at the expense of having to choose specific—namely, spin-glass—types of couplings for the bath.

In order to prevent energy flow from \mathcal{E}_2 into the CS, the environment is prepared in a configuration that resembles a thermal state with inverse temperature $\beta = 50/J_S$, i.e., very close to the GS. Both decoherence and relaxation are sensitive to the precise numerical values of the interaction strengths. The values that are picked lead to efficient decoherence and relaxation for the given size of the environment. The interaction strengths of both models (as well as other parameters) are summarized in Table I.

C. State preparation and simulation procedure

In order to study the decoherence process, it is most instructive to examine a state that is initially unentangled, i.e., a product state. In particular, this work shall encompass the

TABLE I. Model parameters; interaction strengths are expressed in units relative to the exchange constant, J_S , of the central system.

Model A	Model B
$N_S = 6$	$N_S = 4$
$N_{\mathcal{E}} = 8$	$N_{\mathcal{E}_1} = 6$
	$N_{\mathcal{E}_2} = 12$
$I = 20J_S$	$I = 20J_S$
	$I' = 0.1J_S$
	$K = 0.1J_S$
	$\beta = 50/J_S$

decoherence of a CS that is prepared in the GS, $|\psi_0\rangle$, (relative to the model) at time $t = 0$. The global wave function, $|\Psi(t)\rangle$, is then expressed as

$$|\Psi(0)\rangle = |\psi_0\rangle \otimes |\mathcal{E}_0\rangle, \quad (9)$$

with $|\mathcal{E}_0\rangle$ the initial state of \mathcal{E} . The state $|\mathcal{E}_0\rangle$ is constructed using the Box-Muller method [59] to generate a random state. In the case of model B, an additional step is required to turn fragment \mathcal{E}_2 into a thermal-like state. This is done by performing imaginary time evolution $\exp[-\beta H_{\mathcal{E}_2}/2]$ on the random state of \mathcal{E}_2 [60] and subsequent normalization of the resulting wave function.

Time evolution of the global state $|\Psi(t)\rangle$ in model A (B) is governed by the unitary operator $\exp[-itH_A]$ ($\exp[-itH_B]$). Time t shall consistently be expressed in dimensionless form $t = t'J_S/\hbar$, in which t' is dimensionful time and \hbar was restored for clarity. Both real and imaginary time evolutions are numerically calculated by expanding the exponential in Chebyshev polynomials [61,62]. The expansion allows for calculation of the wave function with an accuracy up to machine precision [61,62]. This accuracy is important to unambiguously assign loss of phase coherence to quantum entanglement instead of the accumulation of numerical errors.

Finally, the loss of phase coherence is studied by taking partial traces of the density matrix [63] of the global system $\Pi(t) = |\Psi(t)\rangle\langle\Psi(t)|$. The resulting reduced density matrix (RDM) of the CS is defined as

$$\rho(t) = \text{Tr}_{\mathcal{E}}\Pi(t), \quad (10)$$

where the trace is over all the spin states in \mathcal{E} . For each simulation, a new realization of the environment was generated as well as a new set of random couplings. The data shown here are representative for simulations with different random realizations.

III. COMPARISON OF DECOHERENCE WITH THE QUANTUM ZENO EFFECT

As stated in the introduction, the primary goal is to understand the consequences of repeated local measurement—the local analog of the quantum Zeno effect [1,64]—on antiferromagnets. This section examines to what extent repeated local measurement can be described within the framework of decoherence.

It is intuitively clear that, from the decoherence perspective, a continuous measurement might originate from an environment interacting much longer than the typical timescale of the

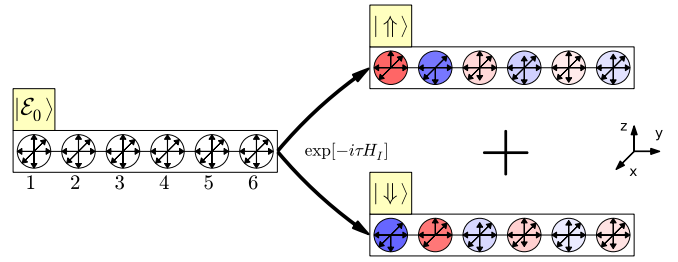


FIG. 2. Pictorial representation of the initial decoherence process in model A. Different parts of the (initial) singlet state evolve to (approximately) orthogonal parts of the environment (denoted by $|\uparrow\rangle$ and $|\downarrow\rangle$) via spin S_1 . The boxes represent a product state of the central system with the environment. The magnetization of each spin is indicated by the arrows, and the red (blue) color intensity illustrates the net magnetization parallel (antiparallel) to the z axis.

CS. One key requirement is that coherences can be quenched locally while maintaining global coherence in the CS. To make the connection between decoherence and the quantum Zeno effect explicit, let us now turn to model A (see Sec. II A) and invoke the Trotter-Suzuki product formula [65],

$$\exp[-itH_A] \approx [\exp(-itH_S^-/n)\exp(-itH_I/n)]^n, \quad (11)$$

in which the approximation becomes exact if n tends to infinity. Under time evolution, the wave function initially branches (partially) due to $\exp[-itH_I/n]$, as different parts of the CS singlet state, $|\psi_0\rangle$, entangle to mutually (close to) orthogonal environment states (see Fig. 2). Subsequently, each branch evolves individually for a time t/n under H_S^- . In comparison, the time evolution according to the quantum Zeno effect is governed by the operator $T_n(t) = [\exp(-itH_S^-/n)P_1^\pm]^n$ with $P_i^\pm = [1 \pm \sigma_i^z]/2$ being the spin S_i projection operator. In the limit where the decoherence timescale τ (the timescale that makes the relative states of \mathcal{E} orthogonal) tends to zero and n tends to infinity, the descriptions $\exp[-itH_A]$ [see Eq. (11)] and $T_n(t)$ become compatible. In this limit, the repeated application of this two-step process causes spin S_1 to be pinned, while the remaining spins in each branch are allowed to evolve freely under H_S^- .

In physically more realistic systems, these precise mathematical limits are never reached. As a result, τ stays finite but small. Therefore, if the Trotter-Suzuki product formula—which has a structure similar to the quantum Zeno time-evolution operator $T_n(t)$ —is used to approximate the evolution operator $\exp[-itH_A]$ with finite $\tau = t/n$, then the contributions coming from the commutator $[H_S^-, H_I]$ as well as higher order commutators are neglected, as can be made explicit using the Campbell-Baker-Hausdorff formula [66].

A. Results model A

The simulation results of model A will now be compared to the quantum Zeno picture, and it will be verified that local decoherence leads to a decoherence wave (DW). The representation $|i_1 \dots i_{N_S}\rangle$ in which each i_k takes the value \uparrow or \downarrow shall henceforth be referred to as the computational basis.

The preceding discussion (and as illustrated in Fig. 2) suggests that coherence in the computational basis between $|\uparrow, i_2, \dots, i_{N_S}\rangle$ and $|\downarrow, j_2, \dots, j_{N_S}\rangle$ diminishes for all

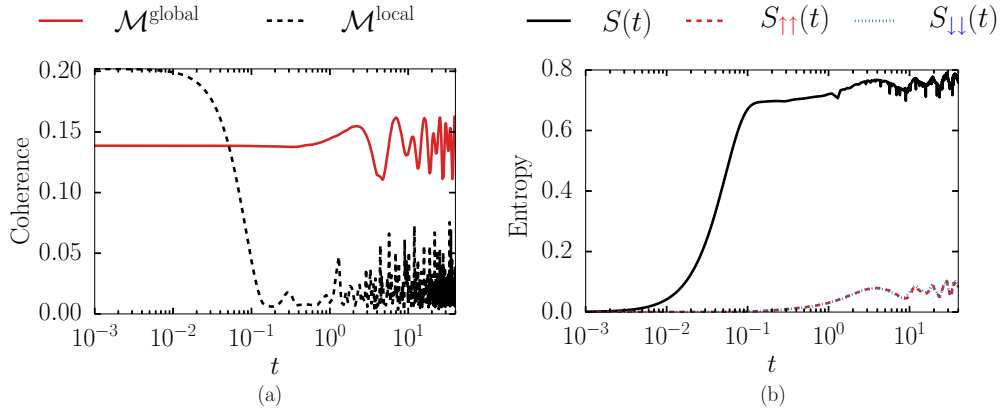


FIG. 3. Simulation results of model A, where spin S_1 of a $N_S = 6$ Heisenberg (open) spin chain is coupled to $N_E = 8$ environment spins via Ising coupling with random uniform interaction strength $I = 20J_S$. The central system is prepared in the (singlet) ground state at $t = 0$. (a) Coherence local to spin S_1 [dashed line, Eq. (14)] and the remainder of the subsystem [solid line, Eq. (15)], as a function of time. Coherence is with respect to the computational basis. (b) Entropy of the entire subsystem $S(t) = S[\rho(t)]$ (solid line) and that complementary to spin S_1 : $S_{\uparrow\uparrow}(t) = S[\tilde{\rho}_{\uparrow\uparrow}(t)]$ (dashed line) and $S_{\downarrow\downarrow}(t) = S[\tilde{\rho}_{\downarrow\downarrow}(t)]$ (dotted line).

realizations of the undetermined indices. At the same time, states with identical S_1^z eigenvalues are expected to be unaffected in the quantum Zeno limit. Therefore, to quantify the local coherence of the RDM

$$\rho_{\{|i_1 i_2 i_3 \dots\}_{j_1 j_2 j_3 \dots\}} \equiv \langle i_1, i_2, i_3 \dots | \rho | j_1, j_2, j_3 \dots \rangle, \quad (12)$$

it is beneficial to focus on the i_1 and j_1 components. To this end, consider the RDM conditioned on the spin S_1 components (as indicated by the bra and ket subscript):

$$\rho_{ab} = {}_1\langle a | \rho | b \rangle_1; \quad \tilde{\rho}_{ab} = \rho_{ab} / \text{Tr}[\rho_{ab}]. \quad (13)$$

Normalization of the density operator $\tilde{\rho}_{ab}$ is primarily to compare entropy, as discussed below. The matrix elements of $\rho_{\uparrow\downarrow}$ (and $\rho_{\downarrow\uparrow}$) determine the degree of (local) S_1 coherence. To measure the loss of local coherence, for each time step t , the maximal magnitude (absolute value) of the $|\rho_{\uparrow\downarrow}|$ components

$$\mathcal{M}^{\text{local}}(t) = \max_{i,j} [|\langle i | \rho_{\uparrow\downarrow}(t) | j \rangle|], \quad (14)$$

is calculated, with $|i\rangle = |i_2, i_3, \dots, i_{N_S}\rangle$ the remaining spins evaluated in the computational basis, and likewise for $|j\rangle$. The coherence of the rest of the CS is determined by the off-diagonal components of $|\rho_{\uparrow\uparrow}|$ and $|\rho_{\downarrow\downarrow}|$, which can similarly be quantified as

$$\mathcal{M}^{\text{global}}(t) = \max_{i \neq j} [|\langle i | \rho_{\uparrow\uparrow}(t) | j \rangle|], \quad (15)$$

where i and j are as above, which do not coincide $i \neq j$ (it must be an off-diagonal component of ρ). The time evolution of the components are shown in Fig. 3(a).

Two regions can be identified: (1) the dephasing regime with $t < 1$ and (2) the dynamic regime $t \sim 1$. Figure 3(a) illustrates that in region 1 the global coherence in the CS is essentially unperturbed while the local coherence associated with spin S_1 is suppressed. Region 2 is determined by the Hamiltonian H_S^- , and it is on this timescale that the DW manifests itself. The oscillatory behaviors of $\mathcal{M}^{\text{local}}(t)$ starting $t \sim 10^0$ are recurrences that originate from the finite size of N_E ; additional suppression can be achieved by increasing N_E .

To further quantify the system's coherence, it is helpful to introduce the von Neumann entropy [67],

$$S[\rho(t)] = -\text{Tr}[\rho(t) \ln \rho(t)], \quad (16)$$

which measures the purity of the density matrix $\rho(t)$ (it vanishes for pure states). Analogously, the entropy of the (normalized) spin S_1 diagonal components of the RDM are defined as $S_{nn}(t) = S[\tilde{\rho}_{nn}(t)]$. In the quantum Zeno description, the diagonal components $\tilde{\rho}_{nn}$ are by definition pure (since it describes wave function collapse, leading to a new pure state). By the normalization of $\tilde{\rho}_{nn}$, this would imply $S_{nn}(t) = 0$. The entropies of the RDM $S(t) \equiv S[\rho(t)]$, as well as $S_{\uparrow\uparrow}(t)$ and $S_{\downarrow\downarrow}(t)$, are shown in Fig. 3(b). What can be seen is that up to $t \approx 1$, the increase in entropy of $\rho(t)$ (tending toward $S = \ln 2 \approx 0.69$) can be primarily attributed to the decoherence of spin S_1 [see also Fig. 3(a)]. For larger times, t , the coherence of the CS is somewhat diminished on a more global scale as the entropy of the spin S_1 diagonal components increase. In addition, the entropy of $\tilde{\rho}_{\uparrow\uparrow}$ is almost the same as that of $\tilde{\rho}_{\downarrow\downarrow}$. This can be understood by noting that, from the local spin perspective, the random environment state looks similar when all the spins are reversed. Simulations, not shown here, indeed indicate that the entropy difference between the two diagonal components varies for each random realization of the environment.

To see how the nonideal aspect, whereby decoherence not only affects spin S_1 but also the remainder of the system, modifies the DW, consider now a time-reversal invariant observable, such as the local energy of the Heisenberg spin chain $\langle S_i \cdot S_{i+1} \rangle$.

In Fig. 4, the nearest-neighbor correlations from the decoherence process are compared to repeated (every $\Delta t = 10^{-1}$) collapse of spin S_1 along the z direction. The latter is achieved by applying the site i projection operator $P_i^\pm = [1 \pm \sigma_i^z]/2$ to the wave function. Although $\langle S_1 \cdot S_2 \rangle$ (left panel of Fig. 4) shows some deviation between decoherence (circular markers) and collapse (thick blue line), the other sites show very good quantitative agreement. The apparent scattering of the $\langle S_1 \cdot S_2 \rangle$ markers actually originates from fast oscillatory behavior.

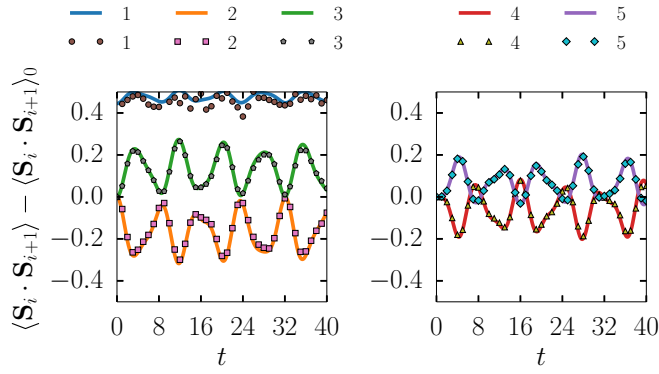


FIG. 4. Nearest-neighbor correlations $\langle \mathbf{S}_i(t) \cdot \mathbf{S}_{i+1}(t) \rangle$ of a $N_S = 6$ antiferromagnetic open Heisenberg chain for different sites i . Repeated collapse (solid lines) along the z direction of spin S_1 (performed every $\Delta t = 10^{-1}$ units of time) is compared with decoherence model A (markers). For clarity, the correlations $\langle \mathbf{S}_i(t) \cdot \mathbf{S}_{i+1}(t) \rangle$ with $i = 1, 2, 3$ ($i = 4, 5$) are shown in the left (right) panel and the $t = 0$ ground-state values, $\langle \mathbf{S}_i \cdot \mathbf{S}_{i+1} \rangle_0 \equiv \langle \mathbf{S}_i \cdot \mathbf{S}_{i+1} \rangle_0$, have been subtracted for each i .

The data points of both the markers and the solid lines are solutions to the Schrödinger equation that are numerically accurate up to machine precision. The deviation between the solutions can therefore be solely attributed to the degree to which the two descriptions are compatible. Further agreement can be achieved by increasing the interaction strength, thereby decreasing the relative importance of the noncommutative contributions and increasing $N_{\mathcal{E}}$ to negate finite-size effects.

It can thus be concluded that even though the description of the decoherence process in terms of the quantum Zeno effect (meaning repeated wave function collapse) is approximate, in practice the two descriptions show a fair degree of compatibility.

IV. STAGGERED FIELD FROM THE QUANTUM ZENO EFFECT

Let us start by discussing the hierarchy of the low-lying excitations in magnetic systems [20,26,35,43,68,69]. The basic tenet is that, in the thermodynamic limit, the collective dynamics (of the antiferromagnet as a whole) are slow compared to the timescale pertaining to the internal excitations that describe local modulations of magnetic order [19]. Hence, the collective configuration—such as absolute position of a crystal or sublattice magnetization direction in an antiferromagnet—can be presumed fixed in comparison to the time interval wherein internal dynamics are relevant [19]. This, of course, still requires that the initial state of the system has a well-defined collective configuration to begin with.

To further discuss the ordering of energy levels, consider the HH [Eq. (1)] in Fourier space (Latin and Greek indices refer to real and Fourier space, respectively) in d spatial dimensions

$$H = J \sum_{\kappa} \gamma_{\kappa} \mathbf{S}_{\kappa} \cdot \mathbf{S}_{-\kappa} = H_{\text{LM}} + J \sum_{\kappa \neq 0, \pi} \gamma_{\kappa} \mathbf{S}_{\kappa} \cdot \mathbf{S}_{-\kappa}, \quad (17)$$

with $\gamma_{\kappa} = \sum_i \cos(\kappa \cdot \mathbf{u}_i)$ a sum over primitive vectors \mathbf{u}_i , and where

$$\mathbf{S}_{\kappa} = \frac{1}{\sqrt{N}} \sum_l e^{i\kappa \cdot \mathbf{R}_l} \mathbf{S}_l, \quad (18)$$

defines the Fourier transform of spin operators \mathbf{S}_l , and \mathbf{R}_l the respective lattice positions (in units of lattice spacing) with periodic boundary conditions. On the right-hand side of Eq. (17), the $\kappa = 0$ and $\kappa = \pi$ contribution are separated to form H_{LM} . On a bipartite lattice H_{LM} turns out to be the Lieb-Mattis [24] Hamiltonian [26,35,43,68,69]

$$H_{\text{LM}} = \frac{4dJ}{N} \sum_{i=1, j=1}^{N/2} \mathbf{S}_{2i-1} \cdot \mathbf{S}_{2j} = \frac{J'}{N} \mathbf{S}_A \cdot \mathbf{S}_B, \quad (19)$$

whereby the odd (even) sites refer to sublattice A (B) and $J' \equiv 4dJ$. For this system, the lowest energy levels are total spin S_{tot} states with maximal S_A and S_B that collapse onto the GS as $J'S_{\text{tot}}(S_{\text{tot}} + 1)/N$ [36,37]. To compare this to the dynamics of H , the complement of H_{LM} can be treated in linear spin wave theory [27]. The “softest” magnon is separated from its ground state as $\propto J/N^{1/d}$, thereby justifying the hierarchy in timescales—in which the collective dynamics are slow compared to the internal magnon excitations—for $d > 1$ (and not too large S_{tot}) in the spin-wave picture [26,35,43,68].

A posteriori analysis of the energy levels of specific systems indicate that the aforementioned dichotomy between collective and local dynamics can indeed be found in many antiferromagnetic systems for $d = 2$ dimensions [35,43,70] not only in near-neighbor antiferromagnets on various lattices [26,43] but also in antiferromagnetic systems with further-neighbor interactions [35,70]. This, then, is another example whereby the emergent physical state is insensitive to the precise microscopic details of the Hamiltonian, as discussed by Laughlin and Pines [17]. Having established that the lowest-lying energy levels of the Lieb-Mattis model approximately describe the respective states of the Heisenberg Hamiltonian (for various lattices and geometries), let us proceed to discuss the consequences of local decoherence. Assume now, for simplicity, that all individual spins (i.e., for both sublattices) are $S_i = 1/2$ and consider the decoherence of spin S_1 positioned on sublattice A . To reiterate, the decoherence of a spin and the quantum Zeno effect are strictly speaking inequivalent. But as demonstrated in Sec. III, in practice the two descriptions are to a large degree compatible. Therefore, assume that spin S_1 is decohered sufficiently strong such that it is, for all practical purposes, pinned along the z direction by its environment.

The branch of the wave function corresponding to spin up (spin down) can now be described by an effective Hamiltonian H_{eff}^+ (H_{eff}^-),

$$H_{\text{eff}}^{\pm} = \frac{J'}{N} \mathbf{S}_{A'} \cdot \mathbf{S}_B \pm \frac{J'}{2N} S_B^z, \quad (20)$$

whereby the spin of the reduced sublattice $\mathbf{S}_{A'} = \sum_{i=2}^{N/2} \mathbf{S}_i$ was introduced. If the initial state of the CS was the GS, belonging to the $S_{\text{tot}}^z = S_A^z + S_B^z = 0$ subspace, the effective Hamiltonian can be cast in the following suggestive form,

$$H_{\text{eff}}^{\pm} = \frac{J'}{N} \mathbf{S}_{A'} \cdot \mathbf{S}_B \mp h_{\text{st}}(S_{A'}^z - S_B^z), \quad (21)$$

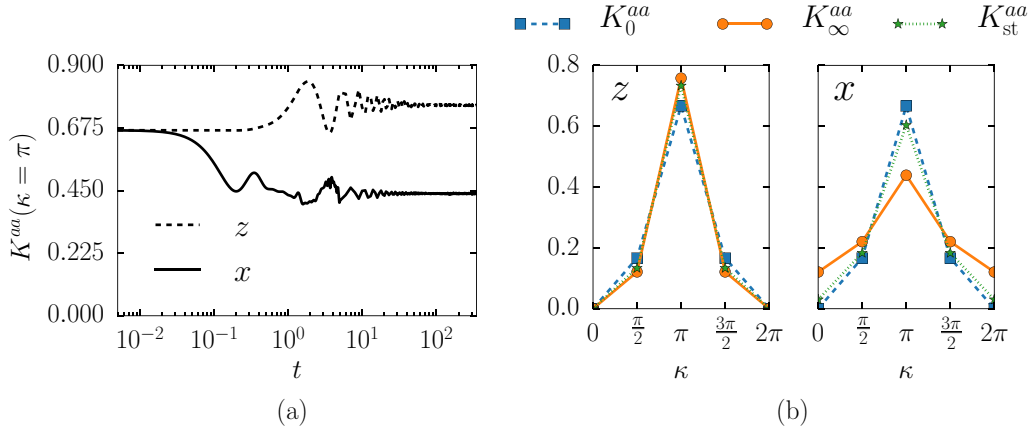


FIG. 5. Simulation data of model B: a $N_S = 4$ antiferromagnetic spin ring, whereby spin S_1 is connected to \mathcal{E}_1 containing $N_{\mathcal{E}_1} = 6$ spins, and the entire central system is in contact with \mathcal{E}_2 , a $N_{\mathcal{E}_2} = 12$ spin state that resembles a thermal reservoir at $\beta = 50/J_S$. \mathcal{E}_1 (\mathcal{E}_2) is Ising coupled to the central system with random uniform (random binary) strength $I = 20J_S$ ($I' = 0.1J_S$), and without (with) intraenvironment coupling (of strength $K = 0.1J_S$). The figures show the static structure factor [see Eq. (22)], whereby the component a is indicated in the panels. (a) Simulation data of the static structure factor evaluated at the antiferromagnetic reciprocal lattice vector (i.e., $\kappa = \pi$) as a function of time. (b) The values of the structure factor in the ground state of the Heisenberg Hamiltonian without [with] an additional staggered field is denoted by $K_0^{aa}(\kappa)$ [$K_{st}^{aa}(\kappa)$] and indicated by square [star] markers. $K_\infty^{aa}(\kappa)$ (filled circles) denotes the simulation data evaluated at $t = 10^3$.

with $h_{st} = J'/(4N)$, whereby an additive constant due to spin S_1 was dropped. Note that in the decoherence framework, time-reversal symmetry is manifestly preserved; the global state of the CS plus environment describes a superposition of two reduced CS (spin S_1 no longer partakes in any dynamics), subject to equal but opposite staggered fields.

V. DEMONSTRATION EMERGENT MAGNETIC ORDER BY DECOHERENCE

To exemplify the dynamic process whereby the decoherence of a local spin enhances antiferromagnetic order by generating a de facto staggered field, consider now model B (Sec. II B). To reiterate, a low-energy description in terms of the Lieb-Mattis model can not be expected to hold for $d = 1$ dimensions, not even approximately. However, writing $\mathbf{S}_A = \mathbf{S}_1 + \mathbf{S}_3$ and $\mathbf{S}_B = \mathbf{S}_2 + \mathbf{S}_4$ shows that the $N_S = 4$ Heisenberg ring (of model B) is special and that it coincides with the Lieb-Mattis model exactly.

A. Results model B

Strictly speaking, the spontaneous breaking of symmetry can only occur in the thermodynamic limit. The results will therefore be compared to an equivalent system that includes a staggered field $H'_S = H_S^\circ + J_S/4M^z$. To quantify the degree of magnetic order, the static structure factor [71]

$$K^{ab}(\kappa) = \langle S^a(\kappa) S^b(-\kappa) \rangle \quad (22)$$

is used, whereby $\kappa = \pi$ corresponds to the antiferromagnetic reciprocal lattice vector on the bipartite chain. In Fig. 5(a), the static structure factor is shown at the magnetic reciprocal lattice. Three different regimes can be identified: (i) $t \sim 10^{-1}$ whereby spin S_1 is decohered by \mathcal{E}_1 resulting in a reduction of $K^{xx}(\pi)$, (ii) $t \sim 1$ with the DW dominating the dynamics as evidenced by the oscillations, and finally (iii) $t > 10$ where

the entire system decoheres due to \mathcal{E}_2 , causing the quantum oscillations to be quenched.

In Fig. 5(b), the magnetic ordering of the decohered system is compared to the GS of H_S° and that of H'_S . The left panel indicates that the enhancement of antiferromagnetic order along the z axis is slightly higher than in the case of a staggered field. On the right panel, one finds that the magnetic order along the x direction is significantly reduced in comparison to the ground state of the Hamiltonian with a staggered field, H'_S . This can be attributed to the small size of the CS, since spin S_1 —which carries significant weight in Eq. (22) for $N_S = 4$ spins—becomes completely uncorrelated along the x axis.

Further support for the claim that the remaining CS is described by the effective Hamiltonian Eq. (21) can be obtained by analyzing $\tilde{\rho}_{nn}$. If this assumption is correct, then, according to decoherence theory [3,72], $\tilde{\rho}_{\uparrow\uparrow}$ ($\tilde{\rho}_{\downarrow\downarrow}$) is expected to become diagonal in $H_{\text{eff}}^{\prime+}$ ($H_{\text{eff}}^{\prime-}$) upon identifying $J'/N = J_S$ and $N = N_S$ (for a detailed discussion of decoherence in the HH, see also Ref. [73]). To measure the loss of coherence in the eigenbasis, for each time step t , the maximum off-diagonal component $|\rho_{n \neq m}(t)|$,

$$\mathcal{M}^{\text{eig}}(t) = \max_{n \neq m} [|\langle E_n | \rho(t) | E_m \rangle|], \quad (23)$$

is calculated. Here, the set $\{|E_n\rangle\}$ refers to the eigenstates of $H_{\text{eff}}^{\prime+}$ ($H_{\text{eff}}^{\prime-}$), the effective Hamiltonian of $\tilde{\rho}_{\uparrow\uparrow}$ ($\tilde{\rho}_{\downarrow\downarrow}$). (Note that coherence is basis dependent; Eqs. (14) and (15) referred instead to the computational basis.) The simulation results are shown in Fig. 6. Decoherence is indeed observed in Fig. 6, thereby corroborating the picture in which local decoherence creates an effective staggered field.

Finally, Figs. 5(a) and 6 indicate a decoherence and relaxation timescale of $t \sim 10^2$ (in dimensionless units) for this model. Using an exchange constant $J \sim 6$ meV, as measured in STM experiments [74] (and ignoring for the moment the presence of magnetic anisotropic terms), estimates that antiferromagnetic order develops in $\tau \sim 10$ ps in model B.

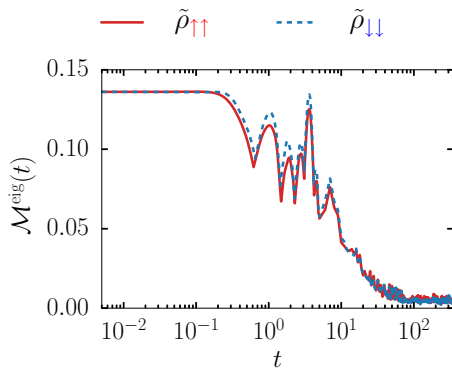


FIG. 6. Loss of phase coherence in model B. The maximum off-diagonal component [see Eq. (23)] of the density matrix $\tilde{\rho}_{\uparrow\uparrow}$ ($\tilde{\rho}_{\downarrow\downarrow}$) is evaluated in the basis diagonalizing H_{eff}^+ (H_{eff}^-).

VI. DISCUSSION AND CONCLUSION

Justification of anomalous fields, that single out the classical symmetry-broken states, was often sought in heuristic arguments. For example, in Ref. [20] it was suggested that thermal disturbances select states with negligible fluctuation in intensive bulk quantities as the only stable low-energy superpositions. Here, the possibility of antiferromagnetic order by repeated local measurement [56] was explored, without the need for a staggered field. Within the decoherence framework, continuous—quantum Zeno—measurement was achieved by rather modest environments, containing as little as seven or eight spin-1/2 particles, and moderately strong environment coupling ($I = 20J_S$ in units of exchange constant J_S). Accordingly, the quantum Zeno picture was applied to a class of isotropic exchange antiferromagnets whereby the low-energy configuration can approximately be described using the Lieb-Mattis (LM) Hamiltonian. To exemplify the enhancement of antiferromagnetic order from the decoherence point of view, the dynamics of a small magnetic structure was analyzed whereby a local spin is strongly coupled to an environment.

A decisive parameter that determines whether sublattices can be pinned is the dimensionality d . From the linear spin wave perspective, the $d \geq 2$ bound follows from the

requirement that the energy levels responsible for symmetry breaking are in the thermodynamic limit well separated from excitations that lead to local modulation of the magnetic order (see also the discussion in Sec. IV). Complementary to this, numerical diagonalization studies of various finite $d = 2$ lattices indicates that the approximate picture provided by linear spin wave theory captures the low-energy behavior of the system surprisingly well [35]. In these cases, the analysis leading to Eq. (21) seems justified, provided that the static structure factor of the system does not vanish [26]. In the $d = 1$ Heisenberg chain, on the contrary, whereby the ground-state spin correlations decay algebraically [75,76], repeated measurements are unable to pin down a sublattice [53]. Only after reducing the quantum fluctuations—by introducing, e.g., anisotropic coupling as done in Ref. [53]—is one able to create quasistable sublattices from a measurement [53]. In this study, magnetic ordering resulted from the decoherence of a small LM magnet, but it is important to note that the staggered magnetization in the LM model is like a classical vector with zero fluctuation [45].

Our exposition is admittedly somewhat artificial from an experimental point of view. One might argue that a system-environment coupling strength of $I = 20J_S$ is unphysically large. But the relevant parameter is the decoherence timescale τ (as discussed in Sec. III), which depends on the interaction strength I , the size of the environment, and possibly other parameters. Thus, I can be small if the environment is sufficiently large. Second, realistic systems usually contain spatially localized impurities or magnetic isotopes that continuously monitor (parts of) the system (see, for example, Ref. [77] for the analysis of nitrogen-vacancy centers in diamond). In this sense, the continuous local measurement strategy is not entirely unrealistic. It is hoped that this work will pave the way toward more realistic descriptions of local decoherence in antiferromagnets.

ACKNOWLEDGMENT

M.I.K. and H.C.D. acknowledge financial support by the European Research Council, Project 338957 FEMTO/NANO.

-
- [1] E. Joos, H. D. Zeh, C. Kiefer, D. J. W. Giulini, J. Kupsch, and I. O. Stamatescu, *Decoherence and the Appearance of a Classical World in Quantum Theory*, 2nd ed. (Springer, Berlin, 2003).
 - [2] W. H. Zurek, *Rev. Mod. Phys.* **75**, 715 (2003).
 - [3] M. A. Schlosshauer, *Decoherence and the Quantum-to-Classical Transition* (Springer, Berlin, 2007).
 - [4] W. Dür and H.-J. Briegel, *Phys. Rev. Lett.* **92**, 180403 (2004).
 - [5] A. R. R. Carvalho, F. Mintert, and A. Buchleitner, *Phys. Rev. Lett.* **93**, 230501 (2004).
 - [6] T. Yu and J. H. Eberly, *Science* **323**, 598 (2009).
 - [7] A. Borrás, A. P. Majtey, A. R. Plastino, M. Casas, and A. Plastino, *Phys. Rev. A* **79**, 022108 (2009).
 - [8] L. Aolita, F. De Melo, and L. Davidovich, *Rep. Prog. Phys.* **78**, 042001 (2015).
 - [9] N. V. Prokof'ev and P. C. E. Stamp, *J. Low Temp. Phys.* **104**, 143 (1996).
 - [10] N. V. Prokof'ev and P. C. E. Stamp, *Rep. Prog. Phys.* **63**, 669 (2000).
 - [11] J.-P. Gauyacq and N. Lorente, *J. Phys.: Condens. Matter* **27**, 455301 (2015).
 - [12] F. Delgado, S. Loth, M. Zielinski, and J. Fernández-Rossier, *Europhys. Lett.* **109**, 57001 (2015).
 - [13] F. Delgado and J. Fernández-Rossier, *Prog. Surf. Sci.* **92**, 40 (2017).
 - [14] A. J. Leggett, S. Chakravarty, A. T. Dorsey, M. P. A. Fisher, A. Garg, and W. Zwerger, *Rev. Mod. Phys.* **59**, 1 (1987).
 - [15] W. Zhang, N. Konstantinidis, K. A. Al-Hassanieh, and V. V. Dobrovitski, *J. Phys.: Condens. Matter* **19**, 083202 (2007).
 - [16] P. W. Anderson, *Science* **177**, 393 (1972).

- [17] R. B. Laughlin and D. Pines, *Proc. Natl. Acad. Sci. USA* **97**, 28 (2000).
- [18] R. B. Laughlin, *A Different Universe: Reinventing Physics from the Bottom Down* (Basic Books, New York, 2006).
- [19] P. W. Anderson, *Concepts in Solids: Lectures on the Theory of Solids*, Frontiers in Physics (W.A. Benjamin, New York, 1964).
- [20] T. Koma and H. Tasaki, *J. Stat. Phys.* **76**, 745 (1994).
- [21] S. V. Vonsovskii and M. S. Svirskii, *JETP* **30**, 140 (1970).
- [22] S. V. Vonsovsky, *Magnetism* (Wiley, New York, 1974), Vol. 2.
- [23] V. Y. Irkhin and M. I. Katsnelson, *Z. Phys. B* **62**, 201 (1986).
- [24] E. Lieb and D. Mattis, *J. Math. Phys.* **3**, 749 (1962).
- [25] H. Jones, *Groups, Representations and Physics* (Taylor & Francis Group, Philadelphia, 1998).
- [26] B. Bernu, C. Lhuillier, and L. Pierre, *Phys. Rev. Lett.* **69**, 2590 (1992).
- [27] P. W. Anderson, *Phys. Rev.* **86**, 694 (1952).
- [28] P. W. Anderson, *Phys. Rev.* **83**, 1260 (1951).
- [29] N. N. Bogolubov, *Phys. (Amsterdam, Neth.)* **26**, S1 (1960).
- [30] M. Oshikawa and I. Affleck, *Phys. Rev. Lett.* **79**, 2883 (1997).
- [31] J. M. Ziman, *Proc. Phys. Soc.* **65**, 540 (1952).
- [32] A. L. Kuzemsky, *Int. J. Mod. Phys. B* **24**, 835 (2010).
- [33] K. Huang, *Statistical Mechanics* (John Wiley and Sons, New York, 2000).
- [34] G. W. Pratt, *Phys. Rev.* **122**, 489 (1961).
- [35] C. Lhuillier, [arXiv:cond-mat/0502464](https://arxiv.org/abs/cond-mat/0502464).
- [36] C. Kaiser and I. Peschel, *J. Phys. A: Math. Gen.* **22**, 4257 (1989).
- [37] T. A. Kaplan, W. von der Linden, and P. Horsch, *Phys. Rev. B* **42**, 4663 (1990).
- [38] F. J. Dyson, E. H. Lieb, and B. Simon, *J. Stat. Phys.* **18**, 335 (1978).
- [39] T. Kennedy, E. H. Lieb, and B. S. Shastry, *J. Stat. Phys.* **53**, 1019 (1988).
- [40] U. Löw, *Phys. Rev. B* **76**, 220409 (2007).
- [41] S. R. White and A. L. Chernyshev, *Phys. Rev. Lett.* **99**, 127004 (2007).
- [42] T. Jolicoeur, E. Dagotto, E. Gagliano, and S. Bacci, *Phys. Rev. B* **42**, 4800 (1990).
- [43] B. Bernu, P. Lecheminant, C. Lhuillier, and L. Pierre, *Phys. Rev. B* **50**, 10048 (1994).
- [44] L. Capriotti, A. E. Trumper, and S. Sorella, *Phys. Rev. Lett.* **82**, 3899 (1999).
- [45] T. A. Kaplan, P. Horsch, and W. Von der Linden, *J. Phys. Soc. Jpn.* **58**, 3894 (1989).
- [46] T. Koma and H. Tasaki, *Phys. Rev. Lett.* **70**, 93 (1993).
- [47] D. N. Astrov, N. B. Ermakov, A. S. Borovik-Romanov, E. G. Kolevator, and V. I. Nizhankovskii, *JETP Lett.* **63**, 745 (1996).
- [48] S. Loth, S. Baumann, C. P. Lutz, D. M. Eigler, and A. J. Heinrich, *Science* **335**, 196 (2012).
- [49] S. Yan, L. Malavolti, J. A. J. Burgess, A. Droghetti, A. Rubio, and S. Loth, *Sci. Adv.* **3**, e1603137 (2017).
- [50] C. F. Hirjibehedin, C.-Y. Lin, A. F. Otte, M. Ternes, C. P. Lutz, B. A. Jones, and A. J. Heinrich, *Science* **317**, 1199 (2007).
- [51] M. I. Katsnelson, V. V. Dobrovitski, and B. N. Harmon, *Phys. Rev. A* **62**, 022118 (2000).
- [52] S. D. Hamieh and M. I. Katsnelson, *Phys. Rev. A* **72**, 032316 (2005).
- [53] H. C. Donker, H. De Raedt, and M. I. Katsnelson, *Phys. Rev. B* **93**, 184426 (2016).
- [54] M. I. Katsnelson, V. V. Dobrovitski, H. A. De Raedt, and B. N. Harmon, *Phys. Lett. A* **318**, 445 (2003).
- [55] M. I. Katsnelson and E. Kogan, *Phys. Rev. B* **72**, 104406 (2005).
- [56] M. I. Katsnelson, V. V. Dobrovitski, and B. N. Harmon, *Phys. Rev. B* **63**, 212404 (2001).
- [57] S. Yuan, M. I. Katsnelson, and H. De Raedt, *Phys. Rev. A* **75**, 052109 (2007).
- [58] S. Yuan, M. I. Katsnelson, and H. De Raedt, *JETP Lett.* **84**, 99 (2006).
- [59] G. E. P. Box and M. E. Muller, *Ann. Math. Statist.* **29**, 610 (1958).
- [60] A. Hams and H. De Raedt, *Phys. Rev. E* **62**, 4365 (2000).
- [61] V. V. Dobrovitski and H. A. De Raedt, *Phys. Rev. E* **67**, 056702 (2003).
- [62] H. De Raedt and K. Michielsen, Computational methods for simulating quantum computers, in *Quantum and Molecular Computing, Quantum Simulations*, Handbook of Theoretical and Computational Nanotechnology Vol. 3, edited by M. Rieth and W. Schommers (American Scientific Publishers, Valencia, USA, 2006), Chap. 1, pp. 2–48..
- [63] U. Fano, *Rev. Mod. Phys.* **29**, 74 (1957).
- [64] B. Misra and E. C. G. Sudarshan, *J. Math. Phys.* **18**, 756 (1977).
- [65] M. Suzuki, *Commun. Math. Phys.* **51**, 183 (1976).
- [66] S. Sternberg, Lie algebras [<http://www.math.harvard.edu/shlomo/>].
- [67] J. Von Neumann, *Mathematical Foundations of Quantum Mechanics* (Princeton University Press, Princeton, NJ, 1955).
- [68] L. Capriotti, *Int. J. Mod. Phys. B* **15**, 1799 (2001).
- [69] J. van Wezel, J. Zaanen, and J. van den Brink, *Phys. Rev. B* **74**, 094430 (2006).
- [70] J. B. Fouet, P. Sindzingre, and C. Lhuillier, *Eur. Phys. J. B* **20**, 241 (2001).
- [71] Y. Zhu, *Modern Techniques for Characterizing Magnetic Materials* (Springer, New York, 2005).
- [72] J. P. Paz and W. H. Zurek, *Phys. Rev. Lett.* **82**, 5181 (1999).
- [73] H. C. Donker, H. De Raedt, and M. I. Katsnelson, *Sci. Post Phys.* **2**, 010 (2017).
- [74] C. F. Hirjibehedin, C. P. Lutz, and A. J. Heinrich, *Science* **312**, 1021 (2006).
- [75] N. M. Bogoliubov, A. G. Izergin, and V. E. Korepin, *Nucl. Phys. B* **275**, 687 (1986).
- [76] J. B. Parkinson and D. J. J. Farnell, *An Introduction to Quantum Spin Systems*, Lecture notes in Physics, Vol. 816 (Springer, Berlin, 2010).
- [77] R. Hanson, V. V. Dobrovitski, A. E. Feiguin, O. Gywat, and D. D. Awschalom, *Science* **320**, 352 (2008).